ACS OMEGA

Open Access

http://pubs.acs.org/journal/acsodf

Article

Gray Frequency-Based Methodology for Assessing Cell Damage

Anqi Li, Linying Zhao, Changyu Liu, Xiaolong Xu,* and Jianbo Jia*

Cite This: *ACS Omega* 2025, 10, 14084−14093

Read Online

ACCESS | Metrics & More | Article Recommendations

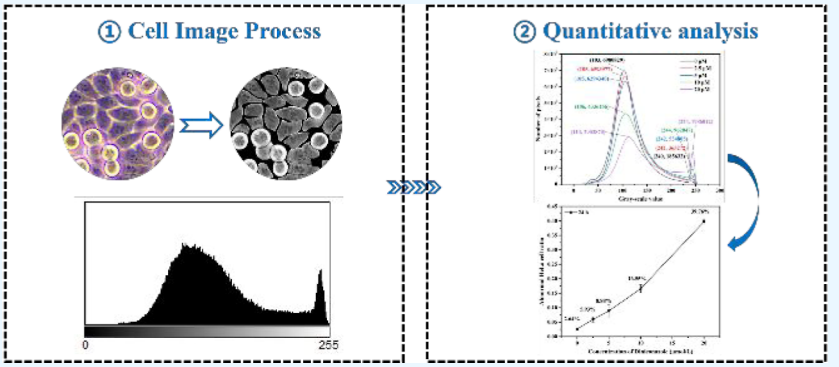

ABSTRACT: Cell biology techniques offer a solid foundation for evaluating and forecasting the danger of pollutants in the investigations of environmental toxicology. Studies on ecological toxicity, medication development, and illness diagnosis depend on evaluating cellular damage. The morphology of stimulated cells can alter the light scattering and reflection, and the brightness of microscopic images of the cells. This study demonstrated that stimulation-damaged and normal cells had distinct gray value distributions which led to the proposal of a novel theory to measure cellular damage by image brightness. Second, various cell types were used to confirm the method's applicability. Additionally, an evaluation technique based on gray frequency analysis can be created to determine the extent of cellular damage. This approach provides an effective and helpful tool for cellular damage visualization and quantitative evaluation in environmental toxicity assessment.

1. INTRODUCTION

With global industrialization and urbanization, the extensive spread of environmental contaminants endangers ecosystems and human health and is a leading cause of sickness and death.[1−3] Cell biology methodologies provide a scientific foundation for analyzing and forecasting contaminant risk in environmental toxicology research. Cell damage assessment is an important component of cell biology methods, which, in addition to being important in disease diagnosis and monitoring[4−6] and drug development and safety assessment,[7−9] is also important in assessing the toxicity of environmental pollutants. Park and Choi discovered that cytotoxicity, genotoxicity, and ecotoxicity tests may accurately assess the possible impacts of environmental contaminants on human health and ecosystems.[10] Rubio et al. found that polystyrene nanoparticles (PSNPs) induce oxidative stress and genetic damage in various human hematopoietic cell lines. The result underscores the importance of conducting cellular damage assays to accurately assess the biological impacts of pollutants, including microplastics.[11] According to Santos et al., the cytotoxicity and genotoxicity of chlorinated disinfection byproducts of 1,3-diphenylguanidine (DPG) confirmed the usefulness of cellular damage assays in the toxicity assessment of environmental pollutants.[12] These findings imply that cellular damage assays not only aid in the rapid screening and identification of harmful compounds but also provide valuable information for understanding the mechanism of action of pollutants.

The most frequent methods for determining the level of cell damage fall into three categories: cell viability assays, biochemical index tests, and morphological observations. Cell viability assays are important for assessing cell survival and function. Kamiloglu et al. discussed a variety of cell viability assays in detail, including staining exclusion (e.g., Taipan blue staining), colorimetric assays (e.g., MTT and MTS assays), fluorescence (e.g., resazurin and 5-CFDA-AM assays), luminescence (e.g., ATP assay), and flow cytometry. (e.g., membrane asymmetry and permeability measurements).[13] Changes in cell viability can directly reflect a cell's response

Received: December 12, 2024
Revised: March 23, 2025
Accepted: March 26, 2025
Published: March 31, 2025

to external stimuli and provide useful information about the level of cellular damage.

Biochemical index assays evaluate various biomarkers and are typically used to estimate cellular damage. Apoptosis tests are an essential part of this category, and the presence of apoptosis is typically determined using methods such as Annexin V-FITC labeling. Apoptosis markers include the production or activation of certain proteins such as cysteine-aspartic proteases (Caspases),[14] cytochrome C,[15] Bcl-2 family proteins,[16] and p53,[17] which can indicate whether a cell is undergoing programmed death. Furthermore, biochemical index testing relies heavily on the detection of oxidative stress indicators. Oxidative stress is a major cause of cellular injury, defined as the breakdown of the equilibrium between oxidants and antioxidants in cells in response to damaging stimuli from the internal and external environments, resulting in cell and tissue damage.[18] This imbalance could be induced by metabolic processes, exposure to toxic chemicals, or a weakened antioxidant system.[19−21] The state of cells under oxidative stress can be determined by measuring intracellular levels of antioxidants (e.g., glutathione GSH) and oxidation products (e.g., malondialdehyde MDA). Changes in these biomarkers can indicate the severity of cellular damage caused by environmental toxins.

Morphological observation assesses cell damage by directly examining changes in cell morphology under a microscope. If there are evident changes in the morphology of the cells following stimulation, such as cell swelling, cell membrane crumpling, and so on, this intuitive information can assist researchers in making a preliminary assessment of the degree of damage. The advantage is that it is intuitive and noninvasive, and morphological changes are typically one of the first responses to hazardous stimuli. Images can reveal changes in cell morphology, making them a valuable tool for analyzing cell damage. Soltanian-Zadeh et al. created an automated approach for segmenting retinal ganglion cells using adaptive optics OCT images that use poorly supervised deep learning. This method increases the accuracy and efficiency of cell damage assessment.[22] Rendeiro et al. used high-parameter imaging mass spectrometry to study the effect of SARS-CoV-2 infection on lung pathology, demonstrating the disordered structure of infected and injured lungs as well as the widespread dispersion of immune infiltrates.[23] This research demonstrated that processing and analyzing cellular pictures can extract damage-related morphological characteristics, which can then be used to measure and quantify cellular damage.

In our investigation, we discovered that microscopic images of normal and stimulated injured cells had different gray scale distributions, indicating a change in brightness between them. Based on this observation, we suggest a novel hypothesis: picture brightness can measure the degree of cellular damage, and a gray scale frequency analysis approach can be created to assess the degree of cellular damage.

2. EXPERIMENTAL SECTION

2.1. Cell Culture and Exposure Conditions. HeLa cells were cultured in a high-glucose culture medium (DMEM) supplemented with 1% penicillin−streptomycin and 10% (v/v) heat-inactivated fetal bovine serum (FBS). After that, they were put in a 37 °C cell culture incubator with 5% CO_2 concentration. After being isolated and suspended in fresh media, HeLa cells in the logarithmic growth phase were subjected to varying doses of diniconazole (2.5, 5, 10, and 20 μmol/L) for a full day.

2.2. Cell Morphology Observation and Photography. HeLa cells in the logarithmic growth phase were collected and transferred to six-well plates with 1×10^6 cells/mL per well. After 24 h of adherence culture, the cells were exposed to 0, 2.5, 5, 10, and 20 μmol/L of diniconazole, and incubated for 24 h. The cell morphology was observed and photographed under an inverted microscope. One hundred photographs were randomly taken for each concentration, and the criteria for taking photographs were that the cells were clearly outlined and that 80% of the area in the photograph was the cellular area.

2.3. Cell Microscopy Image Acquisition and Processing. The treated cells were viewed under a microscope, and high-resolution cell micrographs were taken, which must display the morphological changes and structural properties of the cells under various stimuli. Background segmentation and feature extraction were performed on all acquired microimages to ensure the accuracy of the subsequent analysis, which is briefly detailed below.

2.3.1. Original Picture Capture. Cell samples with varying degrees of damage were prepared and placed in an optical microscope for observation and photography. The magnification of the objective lens was set to 20 times, and the intensity and focal length of the light source were adjusted to ensure that the outlines of the cells were clearly visible in the images to minimize blurring and shadow artifacts.

We rigorously subregion and conduct several trials for every sample group in order to guarantee the correctness and stability of the gray frequency analysis results. In particular, the cell culture plate was separated into four zones, and each zone was randomly photographed. It was made sure that the shooting ranges of the various zones did not overlap. For every concentration, 100 microscopic pictures were captured. Three duplicates of the experiment were conducted.

All experiments were conducted using the same imaging device, light source intensity, focal length, and exposure time to minimize variability caused by imaging conditions.

2.3.2. Image Background Segmentation and Feature Extraction. Cell picture segmentation seeks to separate cells from their surroundings for easier examination. This method employed Cellpose software to boost segmentation efficiency and accuracy. Cellpose is an open-source deep-learning technology developed by Stanford University that can rapidly interpret a wide range of cell pictures.[24] After importing cell micrographs using Cellpose software and its parameter modification tools, the majority of the cells can be segmented automatically, except for a tiny portion that must be segmented manually. Finally, the compressed file can be saved as ROI and loaded into FIJI software for processing, yielding the image after cell segmentation. Finally, the gray value of the target region and the number of associated pixel points were extracted, allowing us to generate the target area's grayscale distribution curve.

2.4. Cell Viability Assay. Cell viability was measured using the CCK-8 kit by the manufacturer's instructions. To conduct cytotoxicity tests, HeLa cells were injected in 96-well plates at a density of 100 μL (5000 cells per well). Diniconazole was added to a final concentration of 0, 2.5, 5, 10, and 20 μmol/L after 24 h of incubation in a cell incubator. After 24 h of incubation, each well received 10 μL of CCK8 solution and

https://doi.org/10.1021/acsomega.4c11226
ACS Omega 2025, 10, 14084−14093

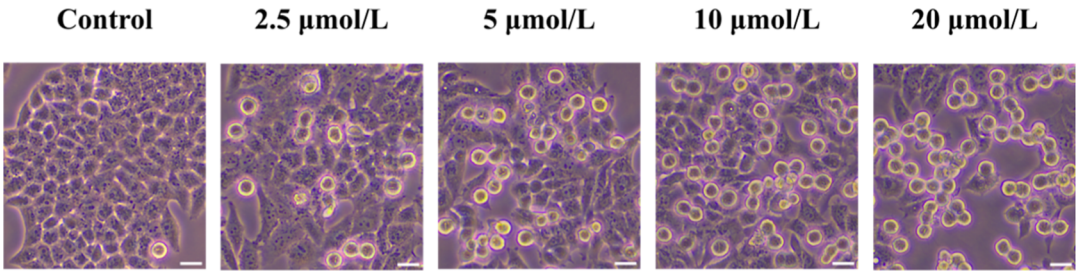

Figure 1. Morphological alterations in HeLa cells after exposure to diniconazole at varied doses (0, 2.5, 5, 10, and 20 μmol/L) over 24 h.

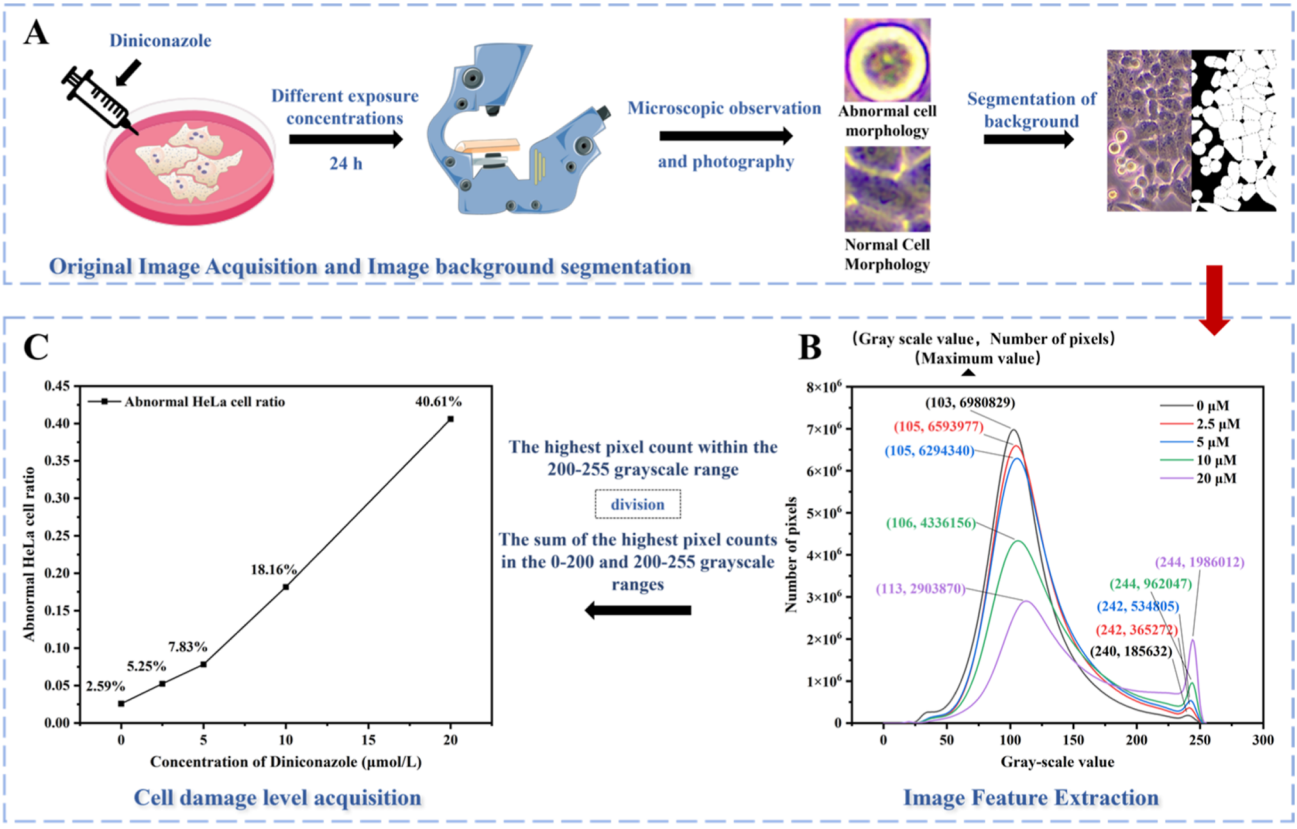

Figure 2. Methodology workflow: (A) schematic of cell image acquisition and processing (syringe, Petri dish, and inverted microscope icons: Bioicons/CC0 1.0; HeLa cell cartoon: DBCLS/Bioicons/CC BY 4.0). (B) Gray curve analysis. (C) Abnormal cell morphology ratio trend. All cell images, segmentation results, and data plots (A−C) are original and authored by the team.

was incubated for 1 h at 37 °C in the dark. Finally, the absorbance was measured at 450 nm using a microplate reader.

2.5. Enzyme and Lipid Peroxidation Assays. The cells were injected onto 6-well plates with 1×10^6 cells per well and incubated for 24 h. The cells were treated with diniconazole at various concentrations (0, 2.5, 5, 10, and 20 μmol/L) and incubated for 24 h. Following incubation, the cells were analyzed for relevant indexes using MDA assay kits, SOD assay kits, and GSH assay kits, as specified by the commercial kit makers. The MDA, SOD, and GSH assay kits should be used according to the manufacturer's instructions. The protein concentration in the cells was measured using the BCA technique.

2.6. Apoptosis Detection. The Annexin V-FITC/PI Apoptosis Assay was used to assess cell death caused by the apoptotic or necrotic pathways. Cells were cultivated in 6-well plates for 24 h before being treated with diniconazole at various concentrations (0, 2.5, 5, 10, and 20 μmol/L). HeLa cells were trypsinized, washed three times with ice-cold PBS, and resuspended in diluted Binding Buffer at a concentration of 1×10^6 cells per mL. Flow cytometry was used to analyze membrane-bound protein V-FITC and propidium iodide (PI) solutions (Beckman Coulter CytoFlex S).

2.7. Evaluation of the Assay's Appropriateness for Various Cell Types. Four cell types—HaCaT, HUVEC, A549, and PC12—were chosen and received a 24 h stimulant treatment with diniconazole. For HaCaT and HUVEC cells, the stimulation concentration gradients were 0, 2.5, 5, 10, and 20 μmol/L; for A549 and PC12 cells, they were 0, 2.5, 5, 10, and 40 μmol/L. Cell viability was measured at each concentration independently, while the equivalent level of cell damage was determined by analyzing the cell's microscopic images.

2.8. Quantifying the Toxicity Severity of Five Triazole Fungicides. Five triazole fungicides, difenoconazole (DIF), penconazole (PEN), bitertanol (BIT), hexaconazole (HEX),

https://doi.org/10.1021/acsomega.4c11226
ACS Omega 2025, 10, 14084−14093

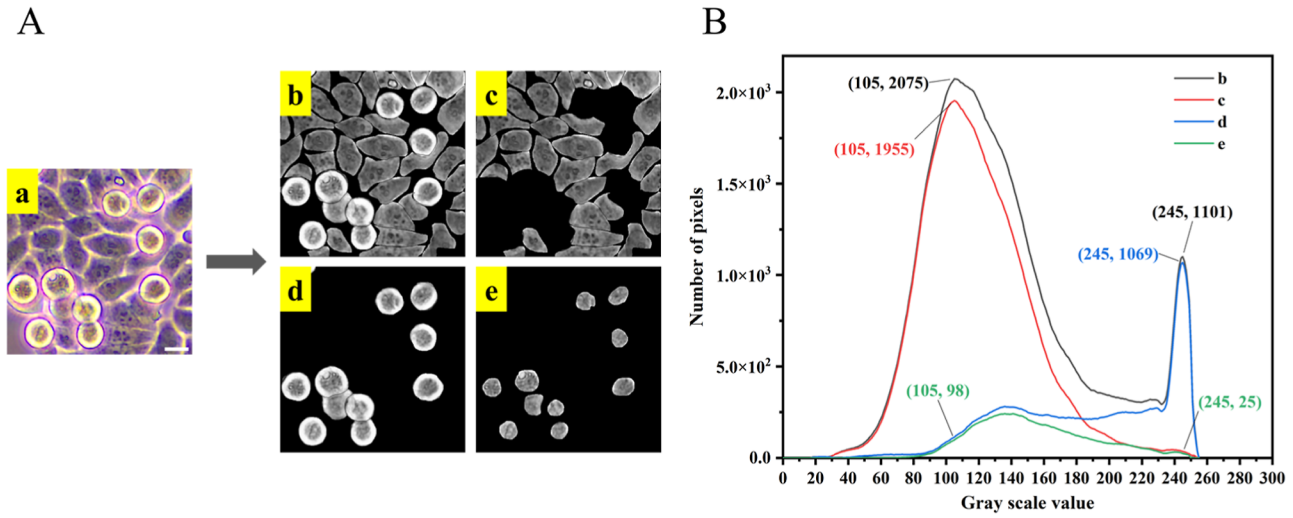

Figure 3. Cell region segmentation results (A), with (a) original image, (b) all cells segmented, (c) normal cells segmented, (d) abnormal cells segmented, (e) darker region of abnormal cells segmented; grayscale curve analysis of different cell regions (B).

and epoxiconazole (EPO), were chosen and tested for toxicity using this technique. Briefly, cells were injected into 6-well plates and cultivated for 24 h. Cells were treated with various triazole concentrations (0, 12.5, 25, 50, and 100 μmol/L) for 24 h. The corresponding microscopic images of the cells were gathered and analyzed, and the degree of damage was assessed.

3. RESULTS AND DISCUSSION

3.1. Effects of Diniconazole on Cell Morphology. After 24 h of exposure to various doses of diniconazole, the HeLa cells were placed under an optical microscope (OLYMPUS CKX53) for cell observation and photography. The morphological alterations of the HeLa cells are depicted in Figure 1. In the control group of HeLa cells, the cells had an oval shape with uniform size, smooth borders, no abnormal protrusions, no evident concave or granular structure, and the interior structure of the cells was visible, with the organelles distributed uniformly. Diniconazole caused the HeLa cells to transform from a uniform oval shape to a round shape, reducing the length-to-diameter ratio and weakening the adhesion force, a phenomenon consistent with cytoskeletal disruption reported for other triazole fungicides.[25−27] The number of cells reduced steadily as the quantity of diniconazole increased. Under the microscope, these round cells were brighter than the surrounding oval or elongated cells. This suggests that diniconazole can cause cell shrinkage by affecting the cytoskeleton, resulting in a reduction in cell size.

3.2. Principle and Construction of Assays. Here we suggest a novel approach to assessing the level of cell damage. This method is built around the frequency of each gray value appearing in the cell photos. The block diagram displayed in Figure 2 depicts the general structure of this method, which can be broken down into two sections: the processing of cell microscope images and the acquisition of the degree of cell damage in two parts.

After 24 h of diniconazole stimulation, cell samples varying in degree of damage were captured on camera and photographed using an optical microscope. The background segmentation of the microscopic images was utilized to identify the region of interest (ROI), from which feature extraction was conducted to ascertain the gray value distribution of the target region's pixels, ultimately yielding corresponding greyscale graphs.

The obtained gray scale graph can be split into two sections, 200−255 and 0−200, as given in Figure 2B. Normal cells are represented by the maximum number of pixel points in the gray scale value 0−200 region, while aberrant cells are represented by the maximum number of pixel points in the gray scale value 200−255 region. We can determine the extent of pollution-induced damage to cells by calculating the ratio of the maximum number of pixel dots in the abnormal region to the total number of maximum pixel dots in the two regions. The percentage of cells with abnormal morphology indicates the extent of cell damage.

Cellular structural disruption, such as increased membrane permeability, organelle disintegration, or decreased density, is frequently observed in damaged cells.[28,29] Because of these alterations, the injured cells look brighter due to increased light scattering, which is easier to see under bright-field viewing.[30,31]

After a specific amount of stimulation, we chose a cell image to confirm the detection method's logic (Figure 3A). Before doing cell segmentation on the image, we first turned it into a grayscale image. The following is the specific content: Initially, we separated each cell in the picture to determine the region's gray curve; Second, the image's cells' normal and aberrant morphologies were separated, and the gray level curves of these two areas were produced. To acquire the gray curve of this region, we finally split the middle portion of the aberrant cells that seemed dark to the human eye. Figure 3B displays the gray curve results. The findings demonstrated a significant difference between normal and abnormal cells' gray values in the distribution corresponding to the appropriate number of pixels. Additionally, the overall effect is insignificant, even if the number of pixels in the black area in the center of the aberrant cell would somewhat interfere with the number of pixels in the normal cell.

This finding suggests that the gray frequency can accurately describe the morphological alterations of cells and offers a natural explanation for the detection method's logic. The ratio of normal to aberrant cells can be measured, allowing for the determination of the extent of cell damage, by analyzing the frequency distribution of the gray values of the two types of

https://doi.org/10.1021/acsomega.4c11226
ACS Omega 2025, 10, 14084−14093

cells. Next, we tested the detection method's viability using HeLa cells as an example.

3.3. Effect of Diniconazole on the Rate of Abnormal Cells. Following a 24 h exposure to varying diniconazole concentrations, microscopic pictures of HeLa cells at the appropriate concentrations were acquired. The related trend graph of the diniconazole content and the ratio of aberrant cells was created by extracting the cell image's gray curve by the procedures outlined in Section 2.3 (Figure 4). The findings demonstrated an increased trend in the ratio of aberrant cells as the diniconazole concentration rose.

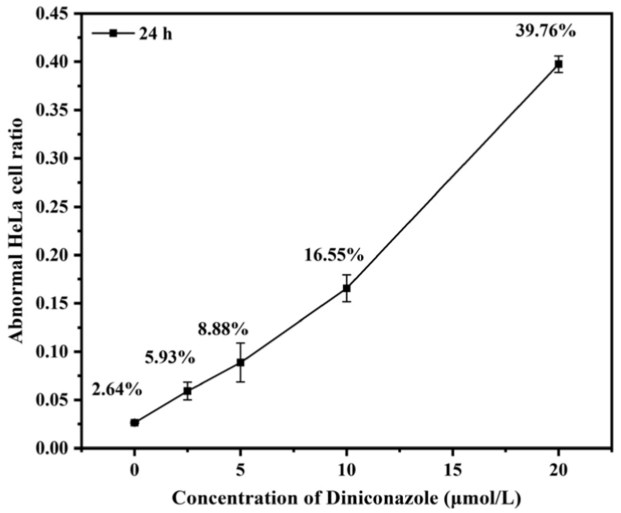

Figure 4. Trend of the proportion of HeLa cells with aberrant morphology. Data are presented as mean ± SD (n = 3).

3.4. Feasibility Analysis. *3.4.1. Effect of Diniconazole on Cell Viability.* Cell viability is an important indicator for determining the degree of cell damage, which refers to the number of cells surviving in a given population, and it is also used to measure the survival or death of cells activated by medications or chemicals.[32] The vitality of HeLa cells was assessed using the CCK-8 cytotoxicity test 24 h after diniconazole was administered, and the findings were presented in Figure 5. The findings in Figure 5 demonstrate

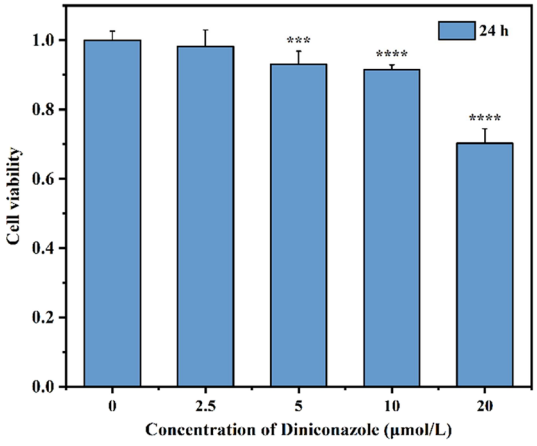

Figure 5. Trend of HeLa cells viability. Twenty-four h after exposure to various concentrations of diniconazole (0, 2.5, 5, 10, and 20 μmol/L). Data are presented as mean ± SD (n = 3). ***p < 0.001 or ****p < 0.0001 when compared with untreated cells.

that there was a negative correlation trend between the viability of HeLa cells and the rise in diniconazole concentration. External stimuli did not affect the cell viability in the control group, which was kept at normal levels. Cell viability did not significantly differ from the control group when stimulated with a low dose of diniconazole (2.5 μmol/L), suggesting that the cells were not significantly affected by this concentration. The viability of HeLa cells decreased as the concentration of diniconazole rose. Diniconazole has a high cytotoxic effect on HeLa cells and is prone to cell damage, as demonstrated by the findings of Xu et al.[33]

3.4.2. Diniconazole Induces Oxidative Stress in HeLa Cells. When oxidants outnumber antioxidants, they disrupt redox signaling and regulation, resulting in oxidative stress.[34] Changes in oxidative stress indicators are intimately related to cell membrane integrity, cellular metabolic activities, and the activation of apoptotic signaling pathways, all of which are significant factors for studying cell injury causes.

As a result, we measured the levels of common oxidative stress indicators in HeLa cells, including MDA, GSH, and SOD. MDA is a common sign of oxidative stress and lipid peroxidation. It is often generated through peroxidation caused by enzymes or free radicals, and it occurs in polyunsaturated fatty acids with at least three double bonds.[35] The body has two major strategies for defending itself against oxidative damage. The first is the scavenging of free radicals by electron donors like GSH, ascorbic acid, and thioredoxin, while the second is the scavenging of free radicals and reactive compounds by enzymes like SOD, catalase (CAT), and glutathione peroxidase (GPx).[36] GSH, for example, acts as a protective barrier against hydrogen peroxide-induced oxidation and is an effective exogenous detoxifier that aids in the reduction of oxidative stress, the maintenance of redox equilibrium, and immune system regulation.[37] SOD is found in many organisms, and its primary function is to catalyze the disproportionation reaction of the superoxide anion (O^{2-}) and convert it into oxygen (O_2) and hydrogen peroxide (H_2O_2), reducing oxidative stress and free radical damage in cells and maintaining the REDOX balance.[38]

We examined the MDA content of HeLa cells after 24 h of exposure to diniconazole at various doses. Figure 6A shows substantial variations in MDA content between the control group and the other three concentrations (except 2.5 μmol/L). Diniconazole can stimulate lipid peroxidation in HeLa cells, promoting an increase in ROS.

Xu et al.[33] discovered that diniconazole can cause ROS in HeLa cells, confirming that diniconazole might cause oxidative stress in these cells. In addition, we investigated SOD enzymatic antioxidants and GSH nonenzymatic antioxidants, both of which play significant roles in controlling oxygen metabolism and free radical harmful effects.[39] In this study, the activities of SOD and GSH in HeLa cells dropped dramatically after 24 h of diniconazole treatment, showing that diniconazole impairs HeLa's ability to remove ROS, resulting in an imbalance between ROS production and breakdown and produces cellular oxidative stress (Figure 6B,C). These findings imply that diniconazole causes excessive ROS, which the cell's antioxidant system cannot adequately eliminate, resulting in oxidative stress and cell damage.

3.4.3. Effect of Diniconazole on HeLa Cells Apoptosis. Apoptosis is a gene-regulated and controlled process of cell death that is required for the maintenance of normal embryonic development and tissue homeostasis in multi-

https://doi.org/10.1021/acsomega.4c11226
ACS Omega 2025, 10, 14084−14093

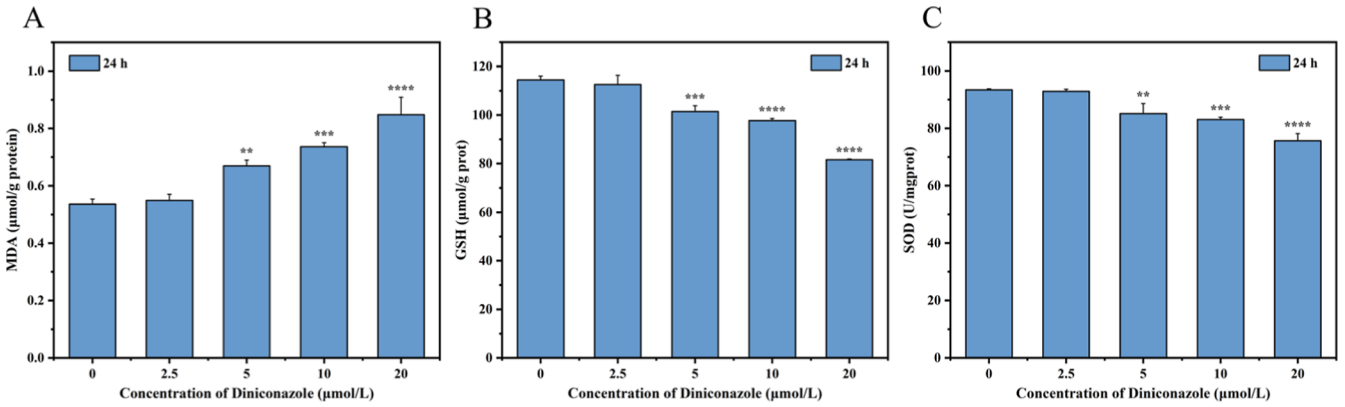

Figure 6. MDA levels (A), GSH activity (B), and SOD activity (C) in HeLa cells exposed to different doses of diniconazole (0, 2.5, 5, 10, and 20 μmol/L) during 24 h. Data are presented as mean ± SD (n = 3). $^{**}p < 0.01$, $^{***}p < 0.001$, $^{****}p < 0.0001$ against untreated cells.

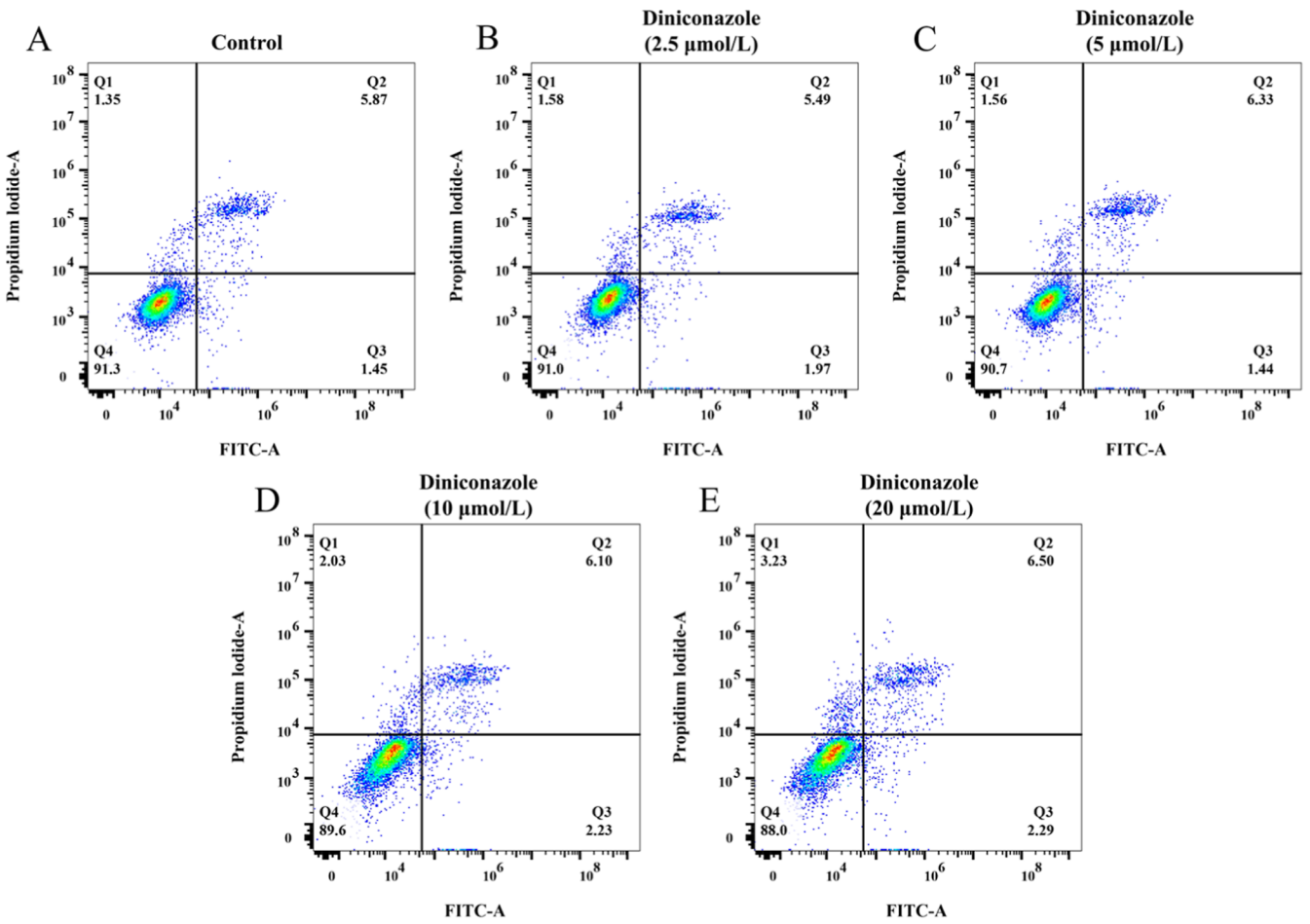

Figure 7. HeLa cell apoptosis following 24 h of exposure to varied concentrations of diniconazole: 0 (A), 2.5 (B), 5 (C), 10 (D), and 20 μmol/L (E).

cellular animals.[40] It is also a crucial physiological mechanism for tissue creation throughout embryogenesis and after birth. Apoptosis is distinguished by cell shrinkage, chromatin concentration, and disintegration into minute membrane-bound apoptotic bodies that are phagocytosed by adjacent parenchymal cells, tumor cells, or macrophages.[41,42] Apoptosis is an important way for cells to deal with injury, therefore it can be used to determine the extent of cell damage. The apoptosis generated by diniconazole was assessed by annexin V-FITC/PI staining. The results showed that when the concentration of diniconazole increased, the number of normal cells decreased somewhat (Figure 7). The precise process by which DIN causes harm to HeLa cells is still unknown. However, it has been reported that HeLa cells stimulated with 80 μmol/L DIN were stained with the AO/EB staining reagent, and the results indicated apoptosis.[33] According to this study, the apoptotic process may have been started by the harmful effects of the unsaturated link in DIN on cells.

3.4.4. Correlation Analysis Using Multidimensional Indicators for Cell Damage. After damage, HeLa cells treated

https://doi.org/10.1021/acsomega.4c11226
ACS Omega 2025, 10, 14084−14093

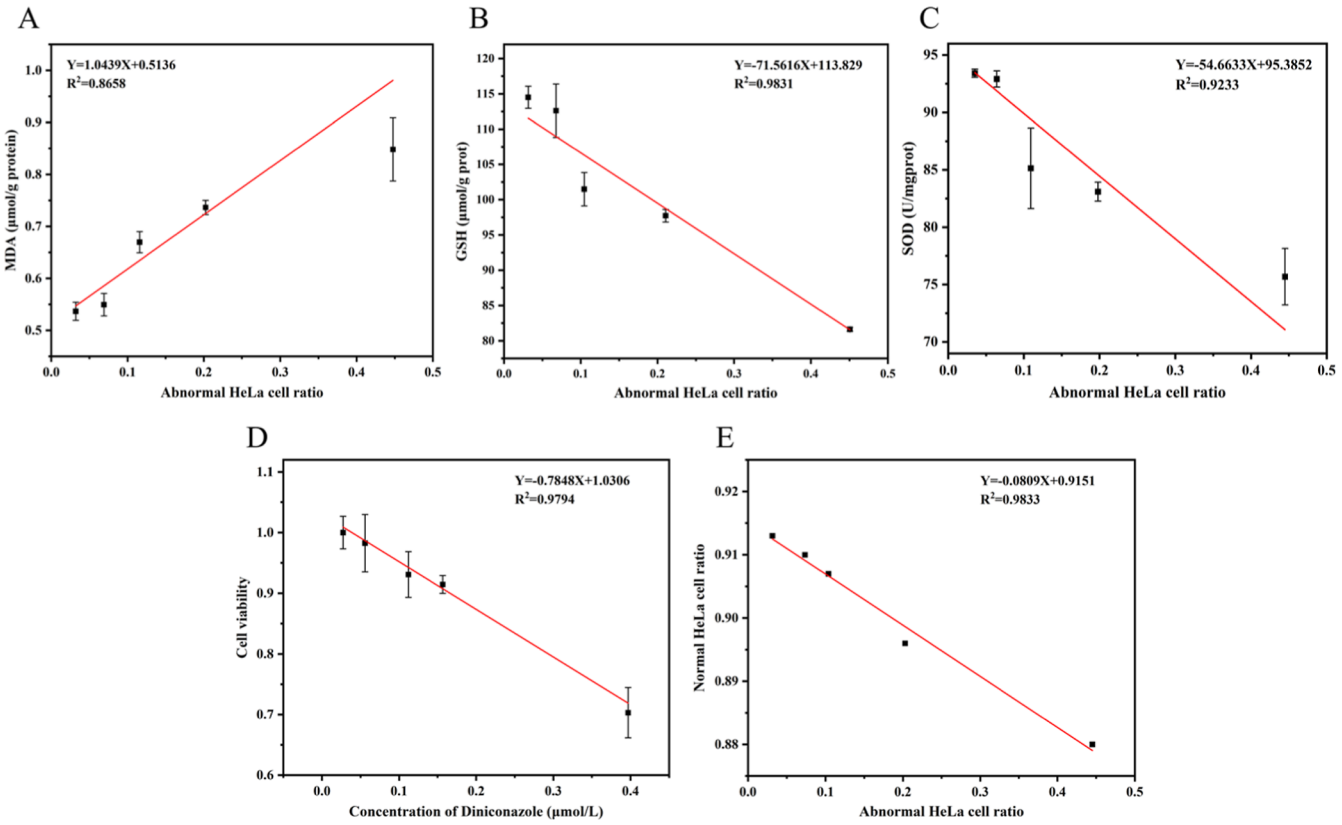

Figure 8. After 24 h of exposure to various concentrations of diniconazole (0, 2.5, 5, 10, and 20 μmol/L), the proportion of HeLa cells with abnormal morphology was fitted to MDA content (A), GSH activity (B), SOD activity (C), cell viability (D), apoptosis (E). The data is shown as the mean ± SD (n = 3).

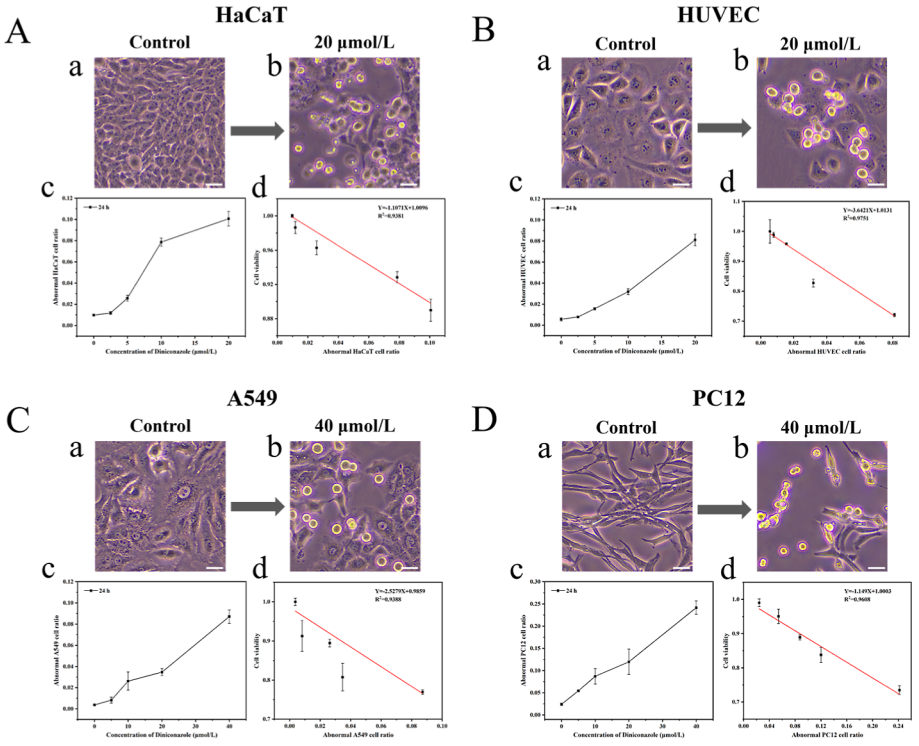

Figure 9. Applicability analysis of the detection method on different cell types: HaCaT (A), HUVEC (B), A549 (C), and PC12 (D). (a) Control and (b) stimulus images of cells exposed to a certain concentration of diniconazole for 24 h; (c) Represents the cell damage degree obtained by the detection method; (d) Represents the fitting analysis between the cell damage degree and cell viability results. The data is shown as the mean ± SD (n = 3).

https://doi.org/10.1021/acsomega.4c11226
ACS Omega 2025, 10, 14084−14093

with diniconazole showed notable changes in morphology and metabolic markers. To assess the efficiency of this method, it is required to compare the cell damage degree acquired by this method, i.e., the fraction of HeLa cells with abnormal morphology, as well as the changes in relevant indicators during the HeLa cell damage process. Figure 8 shows the findings of the comparison analysis. As the proportion of HeLa cells with aberrant shapes grew, the lipid peroxide MDA level increased (Figure 8A), indicating a substantial positive connection. However, cell viability, GSH, and SOD levels, and the ratio of viable cells detected by apoptosis, all decreased as the ratio of HeLa cells with aberrant shapes increased (Figure 8B,−E), indicating a clear negative association. To determine the degree of association between the outcomes determined by the new method and changes in associated markers during HeLa cell damage, linear regression was employed to fit the data. The results revealed that all of the correlation coefficients were greater than 0.8, suggesting a high degree of fit between the extent of cell damage achieved by this approach and the alterations in prevalent cell damage indicators, thereby confirming the method's reliability.

3.5. Assay's Suitability for Several Cell Types was Investigated. Four cell types (HaCaT, HUVEC, A549, and PC12) were chosen in addition to HeLa cells to assess the extent of cell damage induced by varying diniconazole concentrations. Additionally, the viability of corresponding cells at corresponding concentration gradients was assessed (Figure 9). Lastly, an analysis was conducted on the relationship between the degree of cell damage and the cell viability data that were acquired using the detection method. The findings demonstrated that the gray frequency-based detection method's correlation coefficients between the degree of cell damage and cell viability were all over 0.9 in all four cell types, suggesting that the technique is not just appropriate for HeLa cells but also for other cell types.

3.6. Triazole Fungicide Toxicity Detection. We investigated the cellular damage caused by five triazole fungicides: DIF, EPO, HEX, PEN, and BIT. The toxicities of five triazole fungicides were determined using this technique, and the results are shown in Figure 10. Figure 10 displays the five triazole fungicides in descending order of toxicity: DIF, BIT, PEN, HEX, and EPO. The toxicity ranking of the five fungicides produced using this method is similar to the results obtained by Qiao et al. using the toxicological index LC50.[43] By evaluating these five fungicides, we assessed the method's reliability in detecting and differentiating between different toxicity levels, proving its utility and value in the field of environmental toxicology.

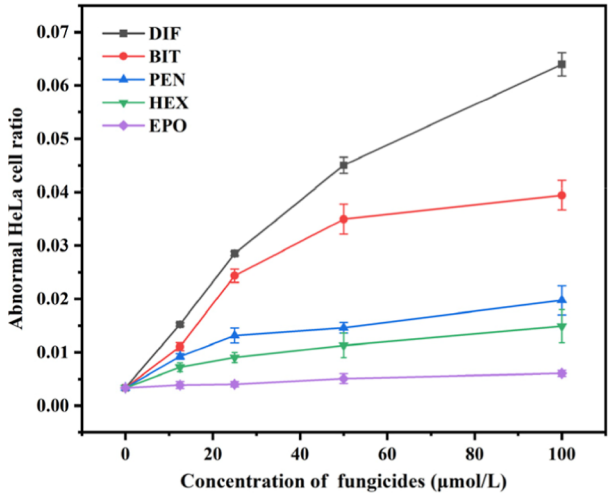

Figure 10. Trend of abnormal morphological ratios in HeLa cells exposed to various concentrations of five triazole fungicides (0, 12.5, 25, 50, and 100 μmol/L) for 24 h. The data is shown as the mean ± SD (n = 3).

4. CONCLUSIONS

In this study, we found that the normal and stimulation-damaged cells had distinct distributions of gray values after the drug stimulation. Based on this, a novel theory was put up, according to which the brightness of an image can indicate the extent of cellular damage. Furthermore, a technique based on gray scale frequency analysis can be created to determine the extent of cellular damage.

In this study, we examined the relationship between the degree of cell damage determined using this technique and the findings of conventional damage indicators to confirm the hypothesis's rationality. To confirm the method's applicability, we simultaneously applied it to various cell types. Lastly, this approach was utilized to measure the toxicity of five triazole fungicides and assess the extent of cell damage; the outcomes were in line with those documented in the literature. This approach offers a useful and promising technique for toxicity assessment of environmental contaminants by combining the visualization and quantitative evaluation of cell damage.

This study is currently in the exploratory phase, with the primary objective of validating the rationality and effectiveness of the grayscale frequency analysis method for assessing cellular damage. While the method may appear relatively cumbersome at this stage due to the limitations of equipment and analysis procedures, this preliminary validation lays a solid foundation for further optimization and automation.

Grayscale frequency analysis has a wide range of potential uses in the future, including environmental toxicity monitoring, anticancer drug screening, and drug toxicity evaluation. This technique can be applied in drug research to assess how organoids or cultured cells react to new substances, which aids in forecasting the safety and adverse effects of medications. It offers a useful technique for screening anticancer treatments to evaluate the effects of various medications on the morphology and damage of cancer cells. Additionally, by examining how contaminants affect organisms in soil samples or water bodies, this method can be used to evaluate the toxicity of environmental pollutants.

In the future, we plan to gradually optimize this method to adapt to automated detection systems, including automated monitoring of cell morphology changes, automated image capturing, and subsequent image processing and analysis. This optimization will significantly enhance detection efficiency, reduce errors from human intervention, and make the method more convenient for large-scale toxicity studies.

AUTHOR INFORMATION

Corresponding Authors

Xiaolong Xu − *Jiangmen Key Laboratory of Synthetic Chemistry and Cleaner Production, School of Environmental and Chemical Engineering; Carbon Neutrality Innovation Center, Wuyi University, Jiangmen 529020, China; Guangdong Provincial Laboratory of Chemistry and Fine*

https://doi.org/10.1021/acsomega.4c11226
ACS Omega 2025, 10, 14084−14093

Chemical Industry Jieyang Center, Jieyang 515200, China; Email: xuxl@wyu.edu.cn

Jianbo Jia − *Jiangmen Key Laboratory of Synthetic Chemistry and Cleaner Production, School of Environmental and Chemical Engineering; Carbon Neutrality Innovation Center, Wuyi University, Jiangmen 529020, China; Guangdong Provincial Laboratory of Chemistry and Fine Chemical Industry Jieyang Center, Jieyang 515200, China;* orcid.org/0000-0003-0671-1527; Email: jbjiagu@163.com

Authors

Anqi Li − *Jiangmen Key Laboratory of Synthetic Chemistry and Cleaner Production, School of Environmental and Chemical Engineering; Carbon Neutrality Innovation Center, Wuyi University, Jiangmen 529020, China*

Linying Zhao − *Jiangmen Key Laboratory of Synthetic Chemistry and Cleaner Production, School of Environmental and Chemical Engineering; Carbon Neutrality Innovation Center, Wuyi University, Jiangmen 529020, China*

Changyu Liu − *Jiangmen Key Laboratory of Synthetic Chemistry and Cleaner Production, School of Environmental and Chemical Engineering; Carbon Neutrality Innovation Center, Wuyi University, Jiangmen 529020, China; Guangdong Provincial Laboratory of Chemistry and Fine Chemical Industry Jieyang Center, Jieyang 515200, China;* orcid.org/0000-0003-2717-3684

Complete contact information is available at: https://pubs.acs.org/10.1021/acsomega.4c11226

Notes

The authors declare no competing financial interest.

■ ACKNOWLEDGMENTS

We acknowledge financial support from the National Natural Science Foundation of China (grant nos. 21974097 and 22274117), Education Department of Guangdong Province (grant no. 2022ZDJS027).

■ REFERENCES

(1) Chowdhury, S.; Pillarisetti, A.; Oberholzer, A.; Jetter, J.; Mitchell, J.; Cappuccilli, E.; Aamaas, B.; Aunan, K.; Pozzer, A.; Alexander, D. A global review of the state of the evidence of household air pollution's contribution to ambient fine particulate matter and their related health impacts. *Environ. Int.* **2023**, *173*, 107835.

(2) Fuller, R.; Landrigan, P. J.; Balakrishnan, K.; Bathan, G.; Bose-O'Reilly, S.; Brauer, M.; Caravanos, J.; Chiles, T.; Cohen, A.; Corra, L.; et al. Pollution and health: A progress update. *Lancet Planetary Health* **2022**, *6* (6), e535−e547.

(3) Mou, Y.; Liao, W.; Liang, Y.; Li, Y.; Zhao, M.; Guo, Y.; Sun, Q.; Tang, J.; Wang, Z. Environmental pollutants induce NLRP3 inflammasome activation and pyroptosis: Roles and mechanisms in various diseases. *Sci. Total Environ.* **2023**, *900*, 165851.

(4) Burton, D. G. A.; Stolzing, A. Cellular senescence: Immunosurveillance and future immunotherapy. *Ageing Res. Rev.* **2018**, *43*, 17−25.

(5) Kamisawa, T.; Zen, Y.; Pillai, S.; Stone, J. H. IgG4-related disease. *Lancet* **2015**, *385* (9976), 1460−1471.

(6) Maria, N. I.; Davidson, A. Protecting the kidney in systemic lupus erythematosus: from diagnosis to therapy. *Nat. Rev. Rheumatol.* **2020**, *16* (5), 255−267.

(7) Fucikova, J.; Kepp, O.; Kasikova, L.; Petroni, G.; Yamazaki, T.; Liu, P.; Zhao, L.; Spisek, R.; Kroemer, G.; Galluzzi, L. Detection of immunogenic cell death and its relevance for cancer therapy. *Cell Death Dis.* **2020**, *11* (11), 1013.

(8) Ingber, D. E. Human organs-on-chips for disease modelling, drug development and personalized medicine. *Nat. Rev. Genet.* **2022**, *23* (8), 467−491.

(9) Weaver, R. J.; Blomme, E. A.; Chadwick, A. E.; Copple, I. M.; Gerets, H. H. J.; Goldring, C. E.; Guillouzo, A.; Hewitt, P. G.; Ingelman-Sundberg, M.; Jensen, K. G.; et al. Managing the challenge of drug-induced liver injury: a roadmap for the development and deployment of preclinical predictive models. *Nat. Rev. Drug Discovery* **2020**, *19* (2), 131−148.

(10) Park, S. Y.; Choi, J. Cytotoxicity, genotoxicity and ecotoxicity assay using human cell and environmental species for the screening of the risk from pollutant exposure. *Environ. Int.* **2007**, *33* (6), 817−822.

(11) Rubio, L.; Barguilla, I.; Domenech, J.; Marcos, R.; Hernández, A. Biological effects, including oxidative stress and genotoxic damage, of polystyrene nanoparticles in different human hematopoietic cell lines. *J. Hazard. Mater.* **2020**, *398*, 122900.

(12) Marques dos Santos, M.; Cheriaux, C.; Jia, S.; Thomas, M.; Gallard, H.; Croué, J.-P.; Carato, P.; Snyder, S. A. Genotoxic effects of chlorinated disinfection by-products of 1,3-diphenylguanidine (DPG): Cell-based in-vitro testing and formation potential during water disinfection. *J. Hazard. Mater.* **2022**, *436*, 129114.

(13) Kamiloglu, S.; Sari, G.; Ozdal, T.; Capanoglu, E. Guidelines for cell viability assays. *Food Front.* **2020**, *1* (3), 332−349.

(14) Sahoo, G.; Samal, D.; Khandayataray, P.; Murthy, M. K. A Review on caspases: Key regulators of biological activities and apoptosis. *Mol. Neurobiol.* **2023**, *60* (10), 5805−5837.

(15) Morse, P. T.; Arroum, T.; Wan, J.; Pham, L.; Vaishnav, A.; Bell, J.; Pavelich, L.; Malek, M. H.; Sanderson, T. H.; Edwards, B. F. P.; et al. Phosphorylations and acetylations of cytochrome c control mitochondrial respiration, mitochondrial membrane potential, energy, ROS, and apoptosis. *Cells* **2024**, *13* (6), 493.

(16) Czabotar, P. E.; Garcia-Saez, A. J. Mechanisms of BCL-2 family proteins in mitochondrial apoptosis. *Nat. Rev. Mol. Cell Biol.* **2023**, *24* (10), 732−748.

(17) Liu, Y.; Gu, W. p53 in ferroptosis regulation: The new weapon for the old guardian. *Cell Death Differ.* **2022**, *29* (5), 895−910.

(18) Sinha, A.; Chu, T. T. T.; Dao, M.; Chandramohanadas, R. Single-cell evaluation of red blood cell bio-mechanical and nano-structural alterations upon chemically induced oxidative stress. *Sci. Rep.* **2015**, *5* (1), 9768.

(19) Gu, Y.; Han, J.; Jiang, C.; Zhang, Y. Biomarkers, oxidative stress and autophagy in skin aging. *Ageing Res. Rev.* **2020**, *59*, 101036.

(20) Hodjat, M.; Rezvanfar, M. A.; Abdollahi, M. A systematic review on the role of environmental toxicants in stem cells aging. *Food Chem. Toxicol.* **2015**, *86*, 298−308.

(21) Zheng, F.; Gonçalves, F. M.; Abiko, Y.; Li, H.; Kumagai, Y.; Aschner, M. Redox toxicology of environmental chemicals causing oxidative stress. *Redox Biol.* **2020**, *34*, 101475.

(22) Soltanian-Zadeh, S.; Kurokawa, K.; Liu, Z.; Zhang, F.; Saeedi, O.; Hammer, D. X.; Miller, D. T.; Farsiu, S. Weakly supervised individual ganglion cell segmentation from adaptiveoptics OCT images for glaucomatous damage assessment. *Optica* **2021**, *8* (5), 642−651.

(23) Rendeiro, A. F.; Ravichandran, H.; Bram, Y.; Chandar, V.; Kim, J.; Meydan, C.; Park, J.; Foox, J.; Hether, T.; Warren, S.; et al. The spatial landscape of lung pathology during COVID-19 progression. *Nature* **2021**, *593* (7860), 564−569.

(24) Stringer, C.; Wang, T.; Michaelos, M.; Pachitariu, M. Cellpose: A generalist algorithm for cellular segmentation. *Nat. Methods* **2021**, *18* (1), 100−106.

(25) Hamdi, H.; Graiet, I.; Abid-Essefi, S.; Eyer, J. Epoxiconazole profoundly alters rat brain and properties of neural stem cells. *Chemosphere* **2022**, *288*, 132640.

(26) Rjiba-Touati, K.; Ayed-Boussema, I.; Hamdi, H.; Abid, S. Genotoxic damage and apoptosis in rat glioma (F98) cell line following exposure to bromuconazole. *Neurotoxicology* **2023**, *94*, 108−116.

(27) Schuster, M.; Kilaru, S.; Steinberg, G. Azoles activate type I and type II programmed cell death pathways in crop pathogenic fungi. *Nat. Commun.* **2024**, *15* (1), 4357.
(28) Dias, C.; Nylandsted, J. Plasma membrane integrity in health and disease: significance and therapeutic potential. *Cell Discovery* **2021**, *7* (1), 4.
(29) Atkin-Smith, G. K.; Poon, I. K. H. Disassembly of the dying: Mechanisms and functions. *Trends Cell Biol.* **2017**, *27* (2), 151−162.
(30) Mourant, J. R.; Freyer, J. P.; Hielscher, A. H.; Eick, A. A.; Shen, D.; Johnson, T. M. Mechanisms of light scattering from biological cells relevant to noninvasive optical-tissue diagnostics. *Appl. Opt.* **1998**, *37* (16), 3586−3593.
(31) Jacques, S. L. Optical properties of biological tissues: a review. *Phys. Med. Biol.* **2013**, *58* (11), R37.
(32) Johansen, J. L.; Sager, T. N.; Lotharius, J.; Witten, L.; Mørk, A.; Egebjerg, J.; Thirstrup, K. HIF prolyl hydroxylase inhibition increases cell viability and potentiates dopamine release in dopaminergic cells. *J. Neurochem.* **2010**, *115* (1), 209−219.
(33) Xu, J.; Xiong, H.; Zhang, X.; Muhayimana, S.; Liu, X.; Xue, Y.; Huang, Q. Comparative cytotoxic effects of five commonly used triazole alcohol fungicides on human cells of different tissue types. *J. Environ. Sci. Health, Part B* **2020**, *55* (5), 438−446.
(34) Sies, H. Oxidative stress: Concept and some practical aspects. *Antioxidants* **2020**, *9* (9), 852.
(35) Demirci-Çekiç, S.; Özkan, G.; Avan, A. N.; Uzunboy, S.; Çapanoğlu, E.; Apak, R. Biomarkers of oxidative stress and antioxidant defense. *J. Pharm. Biomed. Anal.* **2022**, *209*, 114477.
(36) Chandimali, N.; Bak, S. G.; Park, E. H.; Lim, H. J.; Won, Y. S.; Kim, E. K.; Park, S. I.; Lee, S. J. Free radicals and their impact on health and antioxidant defenses: a review. *Cell Death Discovery* **2025**, *11* (1), 9.
(37) Ali, S. S.; Ahsan, H.; Zia, M. K.; Siddiqui, T.; Khan, F. H. Understanding oxidants and antioxidants: Classical team with new players. *J. Food Biochem.* **2020**, *44* (3), No. e13145.
(38) Halliwell, B. Understanding mechanisms of antioxidant action in health and disease. *Nat. Rev. Mol. Cell Biol.* **2024**, *25* (1), 13−33.
(39) Almeida, J. A.; Diniz, Y. S.; Marques, S. F. G.; Faine, L. A.; Ribas, B. O.; Burneiko, R. C.; Novelli, E. L. B. The use of the oxidative stress responses as biomarkers in Nile tilapia (Oreochromis niloticus) exposed to in vivo cadmium contamination. *Environ. Int.* **2002**, *27* (8), 673−679.
(40) Kerr, J. F. R.; Wyllie, A. H.; Currie, A. R. Apoptosis: A basic biological phenomenon with wide ranging implications in tissue kinetics. *Br. J. Cancer* **1972**, *26* (4), 239−257.
(41) Bertheloot, D.; Latz, E.; Franklin, B. S. Necroptosis, pyroptosis and apoptosis: an intricate game of cell death. *Cell. Mol. Immunol.* **2021**, *18* (5), 1106−1121.
(42) Park, W.; Wei, S.; Kim, B.-S.; Kim, B.; Bae, S.-J.; Chae, Y. C.; Ryu, D.; Ha, K.-T. Diversity and complexity of cell death: a historical review. *Exp. Mol. Med.* **2023**, *55* (8), 1573−1594.
(43) Qiao, K.; Fu, W.; Jiang, Y.; Chen, L.; Li, S.; Ye, Q.; Gui, W. QSAR models for the acute toxicity of 1,2,4-triazole fungicides to zebrafish (Danio rerio) embryos. *Environ. Pollut.* **2020**, *265*, 114837.

https://doi.org/10.1021/acsomega.4c11226
ACS Omega 2025, 10, 14084−14093